Transport properties of dense deuterium-tritium plasmas

Cong Wang,[1,2] Yao Long,[1] Xian-Tu He,[1,2] Jun-Feng Wu,[1] Wen-Hua Ye,[1,2] and Ping Zhang[1,2,*]
[1]*Institute of Applied Physics and Computational Mathematics, P. O. Box 8009, Beijing 100088, People's Republic of China*
[2]*Center for Applied Physics and Technology, Peking University, Beijing 100871, People's Republic of China*
(Received 9 February 2012; revised manuscript received 6 June 2013; published 29 July 2013)

Consistent descriptions of the equation of states and information about the transport coefficients of the deuterium-tritium mixture are demonstrated through quantum molecular dynamic (QMD) simulations (up to a density of 600 g/cm^3 and a temperature of 10^4 eV). Diffusion coefficients and viscosity are compared to the one-component plasma model in different regimes from the strong coupled to the kinetic one. Electronic and radiative transport coefficients, which are compared to models currently used in hydrodynamic simulations of inertial confinement fusion, are evaluated up to 800 eV. The Lorentz number is discussed from the highly degenerate to the intermediate region. One-dimensional hydrodynamic simulation results indicate that different temperature and density distributions are observed during the target implosion process by using the Spitzer model and *ab initio* transport coefficients.

DOI: 10.1103/PhysRevE.88.013106 PACS number(s): 52.25.Fi, 51.30.+i, 51.20.+d, 52.65.Yy

I. INTRODUCTION

Inertial confinement fusion (ICF) has been a long-desired goal since the implosion of a capsule of cryogenic deuterium-tritium (DT) covered with a plastic ablator is a visible way to generate a virtually unlimited source of energy [1,2]. In direct-drive ICF, nominally identical Megajoule-class laser beams illuminate the frozen capsule. To trigger the ignition and maximize the thermonuclear energy gain, high compression of the DT fuel and a high temperature of the hot spot should be achieved. In the process of compression, the DT shell accelerates and starts to converge since the laser beams ablate the capsule. The DT shell would experience a wide range of thermodynamical conditions at densities up to several hundreds of a gram per cubic centimeters (g/cm^3) and temperatures from a few to hundreds of electron volts (eV).

Demonstrations of the laser-driven ICF ignition and fusion energy gain in the laboratory are now prepared by the National Ignition Facility (NIF) [3,4]. Understanding and controlling the high-pressure behaviors of DT fuel are of crucial interest for the success of ignition experiments. The equation of states (EOS) of DT fuel are essential for ICF designs because the low adiabat compressibility of the material is dominated by the EOS [5]. During the imploding process, impurities from ablators or hohlraum are inadvertently mixed into the fuel, which strongly influence the burn efficiency and the instability growth near the interface. Thus, the viscosity and diffusion coefficients of the DT mixture are important parameters in hydrodynamic modeling treating interfaces instabilities [6], as well as in further investigating the multiphysical effects of high-Z dopants. Finally, accurate knowledge of the electronic and radiative transport coefficients in dense DT plasmas are also important for precisely predicting all kinds of hydrodynamical instabilities grown at the ablation front, at the fuel-ablator interface, or at the hot-spot–fuel interface, and play central roles in describing the evolution of the central hot spot against the cold fuel [7].

Despite the importance, the thermophysical properties are poorly known, particularly in the hot dense regime. QMD simulations have proven to be powerful tools to study warm dense matter, but are limited in terms of temperatures and densities. For instance, the EOS of hydrogen-helium mixtures were studied at densities between 0.19 and 0.66 g/cm^3 and temperatures from 500 to 8000 K by Vorberger *et al.* [8], then extended to a dense regime ($\rho \sim 6$ g/cm^3) [9]. Morales *et al.* [10] modified the Kerley 2003 EOS through QMD and coupled electron-ion Monte Carlo (CEIMC) simulations, however, the EOS at higher density and temperature still need to be addressed. Recently, the high-density EOS of hydrogen [11] was built by using a two-fluid model combining the quantum Green's function technique for the electrons and a classical description for the ions, and the results agree with QMD calculations in the high density limit. The electronic conductivity was determined for temperatures from 1000 to 50 000 K and equivalent H mass densities of $0.05 \sim 20.0$ g/cm^3 [12,13]. In this work, we focus on the thermophysical properties of the DT mixture at the equivalent H mass density from 80 to 240 g/cm^3 and temperatures up to 10^4 eV for the EOS (800 eV for the electronic transport coefficients).

II. COMPUTATIONAL METHOD

The thermophysical properties of the DT mixture are determined by combinations of first-principles molecular dynamics (FPMD) and orbital-free molecular dynamics (OFMD) [14] using the ABINIT package [15]. In FPMD, electrons are quantum mechanically treated through plane-wave finite temperature density functional theory (FT-DFT) after the introduction of the Born-Oppenheimer approximation. As for OFMD simulations, the orbital-free functional is derived from the semiclassical development of the Mermin functional [16], which leads to the finite-temperature Thomas-Fermi expression for the kinetic part.

Considering the DT mixture at high densities, the Coulombic pseudopotential with short cutoff radius ($r_{\rm cut} = 0.001$ a.u.) has been built to avoid the overlap between pseudocores [17].

*Corresponding author: zhang_ping@iapcm.ac.cn

As a consequence, the large cutoff energy $E_{\rm cut} = 200$ Hartree are used. In this paper, we report QMD calculations for DT mixtures along the 200 to 600 g/cm^3 isochore with Γ point to represent the Brillouin zone and 128 particles in a cubic cell, where FPMD and OFMD are performed up to 100 and 10 000 eV, respectively. We have checked the simulations with respect to a systematic enlargement of the cutoff energy, number of particles, as well as the **k**-point set, and the convergence is better than 5%. Dynamic simulations are carried out from 8000 to 200 000 steps in the isokinetic ensemble [18]. Due to the computational limits of the finite temperature density-functional theory approach, the electronic structure is calculated up to 800 eV, and a $4 \times 4 \times 4$ Monkhorst-Pack k-point mesh is used. In characterizing the plasma states, the ionic coupling and degeneracy parameters have been used. The definition of the first one is $\Gamma_{ii} = Z^{*2}/(k_B T a)$ (the ratio between the electrostatic potential and the kinetic energy), and the later one is $\theta = T/T_F$ (the ratio of temperature to Fermi temperature). The presently studied plasmas goes from strongly coupled ($\Gamma_{ii} \sim 60$) and degenerated states ($\theta \sim 0.01$) to the kinetic states ($\Gamma_{ii} \sim 0.01$ and $\theta \sim 20$).

III. RESULTS AND DISCUSSION

A. Equation of states

Concerning the EOS, the difference between FPMD and OFMD lies within a 2% accuracy below 20 eV, however, as temperature increases, the difference becomes negligible. We have constructed the EOS as polynomial expansions (error within 2%) of the density (200–600 g/cm^3) and temperature (1–10^4 eV) as follows:

$$P = \sum A_{ij} \rho^i T^j, \tag{1}$$

which can be conveniently used in hydrodynamic simulations in ICF or astrophysics (Table I). The present fitted results are only valid at the density-temperature region mentioned above.

Figure 1 shows the calculated EOS as a function of temperature at sampled densities. QMD results are compared to both the ideal and Debye-Hückel models [19]. The pressure of the ideal model ($P_{\rm id}$) can be viewed as the combination of noninteracting classical ions and fermionic electrons. The self-consistent solution of the Poisson equation for a screened charges plasmas leads to the well-known Debye-Hückel model, where pressure can be explicitly expressed as $P_D = P_{id} - \frac{k_B T}{24\pi\lambda_D^3}$. Here λ_D is the Debye length. At a density of 249.45 g/cm^3, the QMD pressures are 9–40% smaller than those given by the ideal model, as temperature lies below 100.0 eV. However, the Debye-Hückel model underestimates the QMD results by 60% at the lowest temperature (2.0 eV) considered. For very high temperatures, beyond T_F, QMD simulation results and the two classical methods merge together into the noninteracting classical ions and electrons (with a difference smaller than 1%). It is clear that the oversimplified ideal or Debye-Hückel model fails to describe plasmas at high density and low temperature. Furthermore, good agreement in EOS is achieved between the present results and other simulation methods, such as the path integral Monte Carlo (PIMC), quantum Langevin molecular dynamics (QLMD), and average atom model with energy-level broadening (AAB) [20–22].

TABLE I. Pressure (kbar) expansion coefficients A_{ij} for Eq. (1) in terms of density (g/cm^3) and temperature (eV).

i	A_{i0}	A_{i1}	A_{i2}
0	671.1939	816.8465	−0.1286
1	12645.2534	753.1419	0.0020
2	151.1943	−0.0401	0.0000

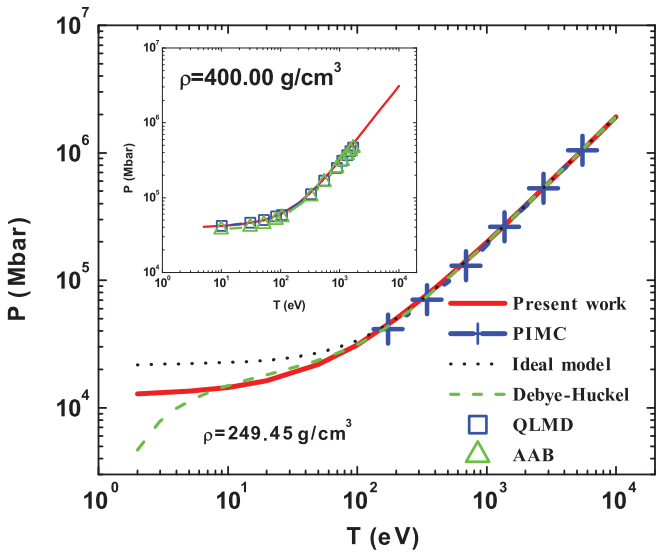

FIG. 1. (Color online) EOS as a function of temperature at 249.45 g/cm^3 (inset is the EOS for $\rho = 400$ g/cm^3). The present QMD results are plotted as red solid lines. Previous results, including the ideal model (black dotted line) and Debye-Hückel model (green dashed line), as well as PIMC (blue cross) [20], QLMD (blue open square) [21], and AAB (green triangle) [22] numerical simulations, are also shown for comparison.

B. Diffusion coefficient and viscosity

Previous QMD simulations in determining the self-diffusion coefficients and viscosity were limited at low densities (equivalent hydrogen mass density up to 8 g/cm^3) and temperatures (10 eV) [23–26]. The present work substantially extends the study on the transport coefficients into a hot dense regime, and comprehensive comparisons with the one-component plasma (OCP) model are described. Here, the self-diffusion coefficient (D) is derived via particle velocity according to the Green-Kubo relation. The viscosity (η) is computed from the autocorrelation function of the five off-diagonal components of the stress tensor: P_{xy}, P_{yz}, P_{zx}, $(P_{xx} - P_{yy})/2$, and $(P_{yy} - P_{zz})/2$. To reduce the length of the trajectory, empirical functions $C[1 - \exp(-t/\tau)]$, where C and τ are free parameters, have been used to fit the integrals of the autocorrelation functions [26]. The fitting procedure is effective in damping the variation and produces reasonable approximations to η (the computed error lies within 10%). Due to the fitting procedure and extrapolation to infinite time, the total error of 20% has been estimated. The uncertainty in the self-diffusion coefficient, where an additional $1/\sqrt{N}$ advantage is secured by particle averages, lies within 2%.

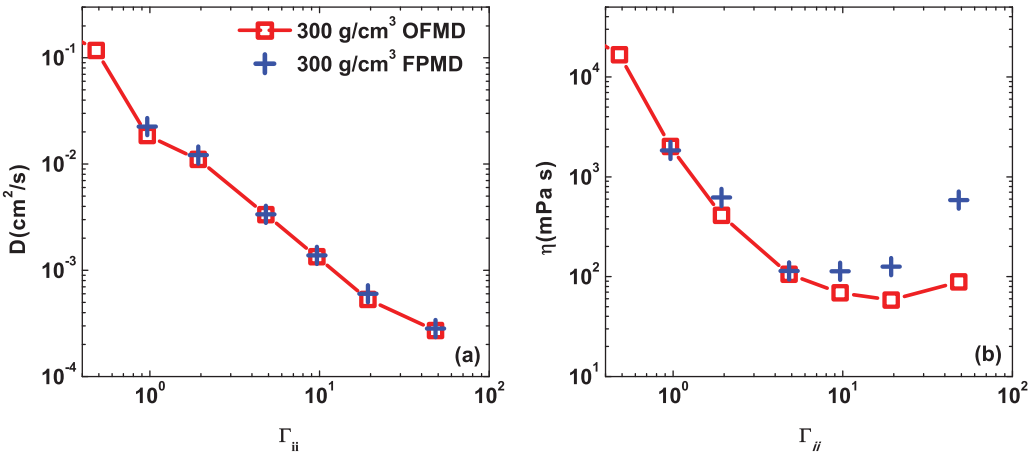

FIG. 2. (Color online) Transport coefficients at a density of 300 g/cm^3 are shown along with coupling parameter $\Gamma_{ii} = \frac{(Ze)^2}{ak_BT}$ (Ze is the ion charge and a the ion-sphere radius). (a) The diffusion coefficients. (b) The viscosity. Results from FPMD and OFMD are denoted by blue cross and red open square, respectively.

The self-diffusion coefficient and viscosity for the DT mixture calculated by FPMD and OFMD as a function of coupling parameter Γ_{ii} at a sampled density of 300 g/cm^3 are shown in Figs. 2(a) and 2(b), respectively. As indicated in the figures, FPMD and OFMD results for self-diffusion coefficients are in generally good agreement (error within 5% or better). As for the viscosity, the divergence between FPMD and OFMD could reach up to ∼70% at low temperatures, however, as temperature increases, they tend to merge together. To compare these results with OCP simulations conveniently, the self-diffusion coefficient D and viscosity η are reduced to a dimensionless form: $D^* = D/\omega_p a^2$ and $\eta^* = \eta/n_i M\omega_p a^2$, where $\omega_p = (4\pi n_i/M)^{1/2}Ze$ is the plasma frequency for ions of mass ($M = 2.5$ amu.). A memory-function analysis of the velocity autocorrelation function has been used to obtain the diffusion coefficient of OCP ($D^* = 2.95\Gamma^{-1.34}$), however, this result is not accurate at $\Gamma \leqslant 4$ [27]. Recently, a more accurate fit (valid at $0.5 \leqslant \Gamma \leqslant 200$) to the OCP simulations has been provided by Daligault [28]. Yukawa models have also been applied to simulate the transport properties for particles moving through the screened Coulomb potential in the strongly coupled region ($\Gamma > 1$) [29,30]. In Fig. 3(a), we compare OFMD data with those OCP and Yukawa (with $\kappa = 0.1$) [31] simulations. The general feature of our simulation result agrees with that of Hansen *et al.* [27] and Ohta *et al.* [29], but visible divergence (3–50%) is still observed. The accordance of the Daligault's fit with the present results is better at low temperatures. With increasing temperature, the Daligault's OCP fitting overestimates the OFMD results by ∼40% at $\Gamma_{ii} = 0.5$. The present results for the reduced viscosity are shown in Fig. 3(b), where the results from OCP and Yukawa simulations are also provided for comparison. By performing classical molecular dynamics of OCP, Bastea [32] fit η^* to the form $\eta^* = 0.482\Gamma_{ii}^{-2} + 0.629\Gamma_{ii}^{-0.878} + 0.00188\Gamma_{ii}$. The

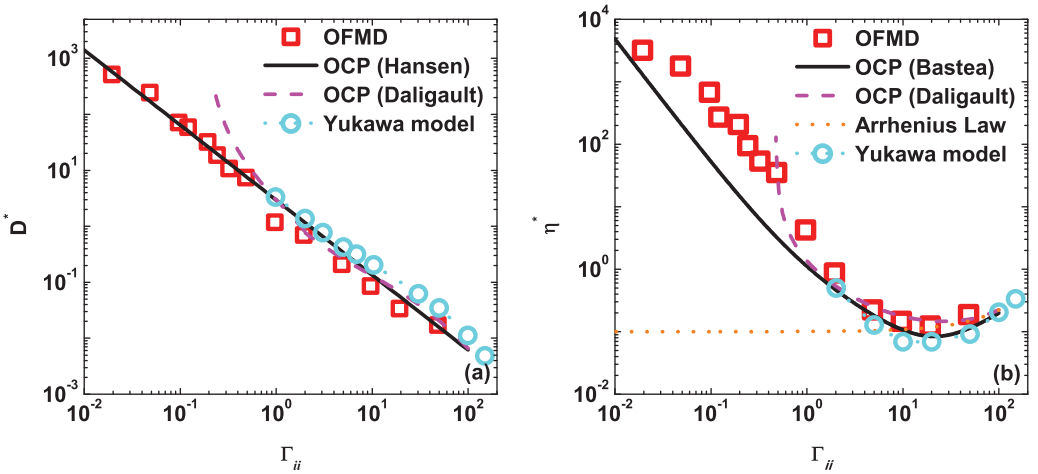

FIG. 3. (Color online) The reduced transport coefficients are shown along with coupling parameter Γ_{ii}. (a) The reduced diffusion coefficients: Present OFMD simulation results at a density of 300 g/cm^3 are plotted as red open squares. OCP results obtained by Hansen *et al.* [27] and Daligault [28] are denoted by black solid line and magenta dashed line, respectively. The Yukawa [31] diffusion coefficients are shown as cyan open circles. (b) The reduced viscosity, where results from OCP (Bastea [32]) and Arrhenius law are plotted as black solid line and orange dotted line, respectively. Other symbols in (b) have the same meaning as those in (a).

present simulation results for viscosity indicate a similar behavior between dense plasma and normal fluid, that is, both of the movement of particles and the action of interparticle forces contribute to the transport of momentum. At large coupling, the viscosity increases with decreasing temperature (or adding density), where an Arrhenius-type relation ($\eta^* = 0.1 \times e^{0.008\Gamma_{ii}}$) is observed. At the intermediate region, $10 \leqslant \Gamma_{ii} \leqslant 50$, contributions from the two mechanisms vary with similar magnitude, leading to a shallow minimum. OCP simulations indicate that the minimum lies at around $\Gamma_{ii} = 25$ [28], while our FPMD and OFMD results suggest the minimum near $\Gamma_{ii} = 11$ and $\Gamma_{ii} = 15$, which are accordant with Yukawa simulations [30]. When $\Gamma_{ii} < 10$, as in a gas, the movement of particles is predominant and the viscosity increases with temperature. Classical models such as OCP and Arrhenius law are not expected to work well for hot dense plasmas.

C. Electronic and radiative transport coefficients

Apart from the EOS and ionic transport coefficients, the electronic transport coefficients are derived using QMD in the following steps. Ten snapshots are directly taken from FPMD equilibrium trajectories up to 100 eV, however, beyond this value, the structures are extracted from OFMD simulations. Then the dynamical conductivity $\sigma(\omega) = \sigma_1(\omega) + i\sigma_2(\omega)$ is evaluated through the Kubo-Greenwood formula as averages of the selected configurations. The dc conductivity ($\sigma_{\rm dc}$) follows from the static limit $\omega \to 0$ of $\sigma_1(\omega)$. In the Chester-Thellung version [33], the kinetic coefficients $\mathcal{L}_{ij}$ are described as

$$\mathcal{L}_{ij} = (-1)^{i+j} \int d\epsilon \hat{\sigma}(\epsilon)(\epsilon - \mu)^{(i+j-2)} \left(- \frac{\partial f(\epsilon)}{\partial \epsilon} \right), \quad (2)$$

with $f(\epsilon)$ being the Fermi-Dirac distribution function and μ the chemical potential. The electronic thermal conductivity K_e is given by

$$K_e = \frac{1}{T} \left(\mathcal{L}_{22} - \frac{\mathcal{L}_{12}^2}{\mathcal{L}_{11}} \right). \quad (3)$$

The electronic heat conduction as a function of temperature along the isochore of 200 g/cm^3 up to 800 eV is shown in Fig. 4(a). The results from theoretical models, which are currently used in hydrodynamics simulations for ICF, as well as previous *ab initio* simulations, are provided for comparison. The Hubbard model [34] is valid for a highly degenerate electron system, where the electronic states are treated by using independent plane waves. The interactions between nuclei are not screened by electrons, and atomic configurations are assumed to be Debye- or OCP-like. Unfortunately, thermal conditions in ICF often enter the partially degenerate regime, which clearly goes beyond the hypothesis of the Hubbard model. The Lee-More model [35], which is not quite accurate in the degenerate state, uses different formulas for the electron collision time in a solid, liquid, and plasma. The Spitzer model [36], which exhibits a power law on the temperature ($T^{5/2}$), has been dedicated to kinetic plasmas, and is not suitable for the dense plasmas considered in this work. At high temperatures, our QMD results and Lee-More model merged together into the Spitzer conductivity. From the quantum Boltzmann equation coupled with Ziman theory, Ichimaru [37] derived hydrogen transport coefficients restricted to the moderate coupling $\Gamma < 2$. From Fig. 4, clearly, the Ichimaru model results overestimate the present data (up to ~30%) at the strong coupled regime, and then the difference reduces to 10%. Remarkably, our QMD data of the electronic thermal conductance for DT mixtures show reasonable consistency with the recently developed self-consistent average-atom model (SCAALP) [38] and previous QMD simulations for hydrogen [7,39] in a wide range.

The results for $\sigma_{\rm dc}$ are presented and compared to those obtained by classical models or *ab initio* simulations in Fig. 4(b). It has been demonstrated that the Hubbard model recovered the Wiedemann-Franz low in the degenerate limit, and thus the electrical conductance are computed from the thermal conductance. For the Spitzer model, the electrical conductivity is obtained by using the Lorenz number at the lower limit of kinetic matter including *e-e* collisions. Our QMD results agree well with the Ichimaru model [37] and data by Lambert *et al.* [14] in a wide region between the degenerate state and the kinetic state.

The thermal conductance and the dynamic conductivities are calculated so as to examine the Lorenz number defined as

$$L = \frac{K_e}{\sigma_{\rm dc} T} = \gamma \frac{k_B^2}{e^2}. \quad (4)$$

The nature of the screened potential, which is responsible for the scattering of the electrons, determines γ. L is constant in the degenerate and coupled state (γ is equal to $\pi^2/3$), reducing to the ideal Sommerfeld number. In the nondegenerate case, γ reaches 1.5966 considering *e-e* collisions. In the intermediate degenerate region, it is difficult to deduce the electronic thermal conductivity from electrical conductance by Wiedemann-Franz law due to the fact that there exists no assumption on the γ value. In Fig. 5(a) we show the γ value as a function of the degeneracy parameter θ for different densities. The simulation results indicate that the Lorenz number oscillates around the Sommerfeld limit in the degenerate region. As θ increases, the departure of the Lorenz ratio from the ideal value towards the lower limit is observed.

Another useful coefficient, which plays an important role in the energy transport formulation of ICF and astrophysics, is the radiative thermal conductivity (K_r). As usual, it is connected to the Rosseland mean path length ($l_R = \frac{1}{\rho \kappa_R}$ with κ_R the Rosseland mean opacity, RMO) by the following relation [1]:

$$K_r = \tfrac{16}{3} \sigma_B l_R(\rho, T) T^3, \quad (5)$$

where σ_B is the Stefan-Boltzmann constant. In particular, the RMO can be in the form

$$\frac{1}{\kappa_R} = \int_0^\infty \frac{B'(\omega)}{\alpha(\omega)} d\omega, \quad (6)$$

where $B'(\omega)$ is the derivative with respect to the temperature of the normalized Plank's function. $\alpha(\omega) = \frac{4\pi}{n(\omega)} \sigma_1(\omega)$ is the absorption coefficient with $n(\omega)$ the real part of the index of refraction. A comparison for K_r is made in Fig. 5(b) between our QMD simulations and those given by fully ionized plasma and the Dyson limit. Zeldovich and Raizer have proven that [40] the RMO of fully ionized plasma can be obtained as $\kappa_R^{\rm ideal} = 0.014(Z^3/A^2)\rho(k_B T)^{-7/2}$ cm^2/g. In this relation, Z is the atomic number, A is the atomic

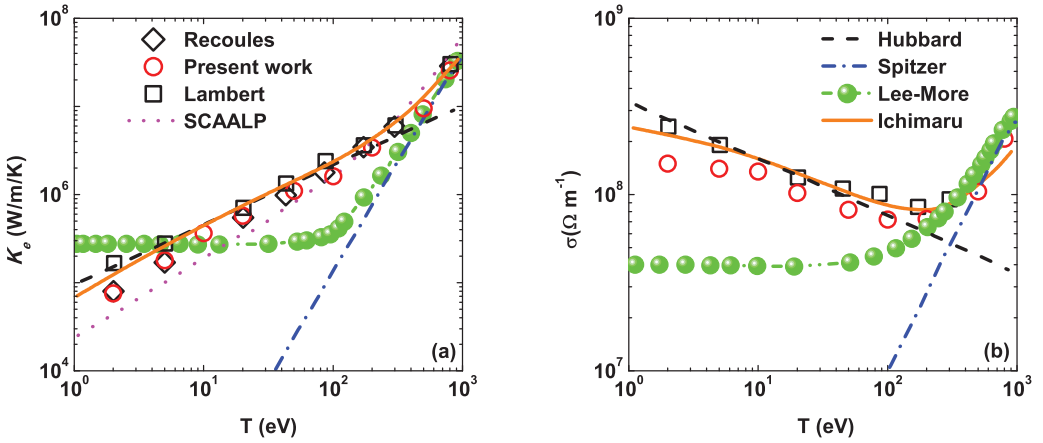

FIG. 4. (Color online) (a) Electronic thermal conductivity of the present work (red open circle) has been compared with previous QMD simulations from Recoules *et al.* (black open diamond) and Lambert *et al.* (black open square) [7,39], and the results from classical models are also shown, such as Hubbard (black dashed line) [34], Spitzer (blue dash dotted line) [36], Lee-More (green solid circle) [35], Ichimaru model (orange solid line) [37], and SCAALP (magenta dotted line) [38]. (b) Electrical conductivity, where the present results are shown with red open circle [other symbols and lines are the same with those in (a)].

weight, and k_BT is expressed in kilo-eV. The upper limit of RMO [$\kappa_R \leqslant 6.0 \times 10^3 Z/(Ak_BT)$ cm^2/g] has been reported by Bernstein and Dyson via applying Schwartz's inequality to a particular factoring of the integrand in the definition of RMO [41]. Our QMD simulation results indicate that K_e governs the energy transport process in the fully degenerate state. As the matter enters the moderate degenerate case, K_r rises about four orders of magnitude as the temperature increases from $\sim 10^2$ eV to $\sim 10^3$ eV, and becomes dominant when θ exceeds ~ 0.5.

D. Applications to ICF

Since the behavior of the electronic thermal conductivity from *ab initio* simulations is quite different from those models, such as the Hubbard model and Spitzer model, as a consequence, one fitted formula for K_e in terms of ρ (in g/cm^3) and T (eV) has been built and applied to investigating ICF target implosions:

$$K_e(\rho,T) = (P_1 + P_2\rho)T^{5/2} + \left(P_3 + P_4\Gamma + P_5 \ln(T)\frac{1}{1+\exp(\theta)}\right)\rho T, \quad (7)$$

with $P_1 = 0.5135$, $P_2 = 0.0006$, $P_3 = 522.4466$, $P_4 = 8.1557$, and $P_5 = -23.5396$. The current K_e model considers a Hubbard-like behavior at the electronic degenerate region and merges to the Spitzer model at an extremely high temperature. In the partially degenerate region, ionic coupling and electronic degenerate parameters are also introduced in the formula to present the complex behavior of the nonideal plasmas.

To study the influence introduced by K_e in ICF implosions simplified one-dimensional single temperature hydrodynamic simulations are performed, where the results are compared by using K_e from QMD simulations and the Spitzer model. Using radiation-hydrodynamics codes (one-dimensional

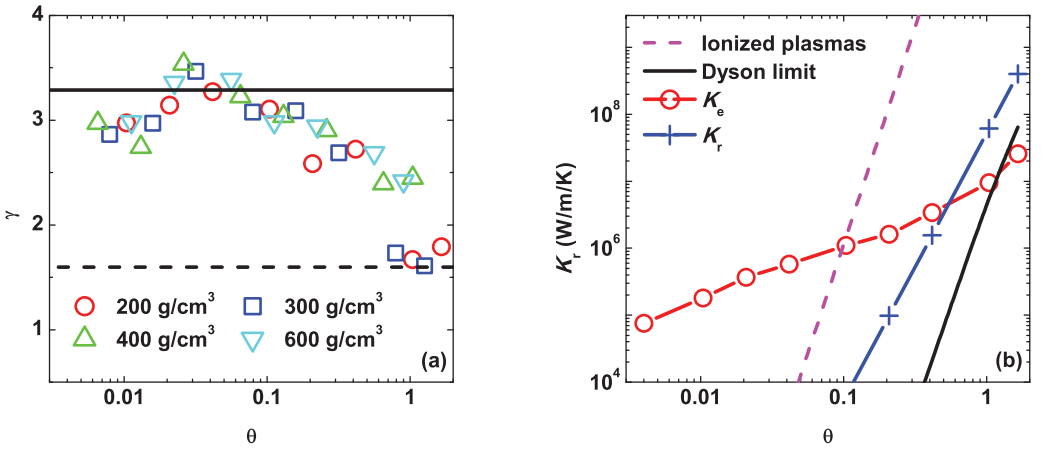

FIG. 5. (Color online) (a) At densities of 200 (red open circle), 300 (blue open square), 400 (green up triangle), and 600 (cyan down triangle) g/cm^3, Lorentz numbers (γ) have been shown as a function of the degenerate parameter θ. (b) Radiation thermal conductivity (K_r) along θ: QMD results are denoted by blue cross; results from Dyson limit and fully ionized plasmas are plotted as black solid line and magenta dashed line, respectively; The electronic thermal conductivity is presented with red open circle.

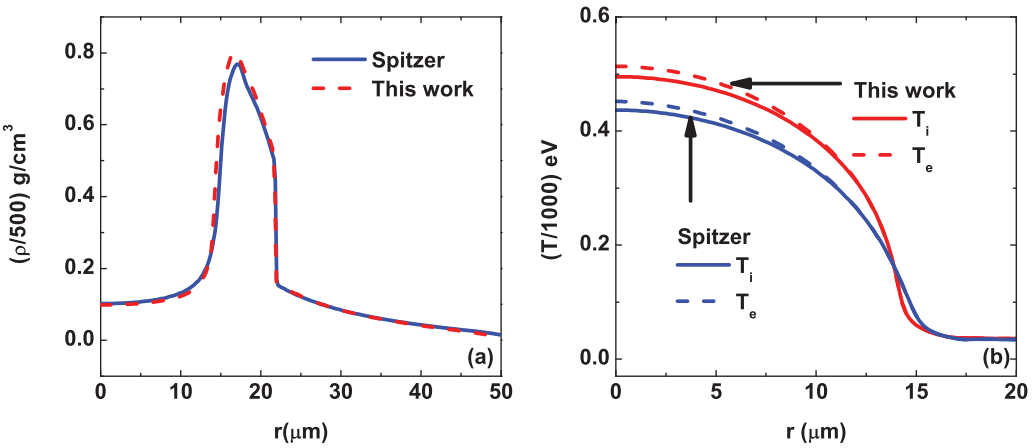

FIG. 6. (Color online) Results for the (a) density and (b) temperature distribution along the radius of the DT capsule [comparison between the Spitzer model and the present *ab initio* model Eq. (7)].

LARED-S [42]) for simulations of target implosions, we have explored the implications of the *ab initio* electronic transport coefficient for designing and understanding the ICF implosions. In the present hydrodynamic simulations, the standard flux-limited ($f = 0.06$) thermal transport model is used and a direct-drive implosion is considered, where the DT capsule is exposed to be illuminated through the laser pulse shapes consisting of a prepulse (with the power of 0.75 TW for 1.6 ns) and the main pulse (with the power of 33.0 TW for 0.75 ns). The cryogenic DT target (360-μm radius) has a 10-μm ablator (hydrocarbon) and 100-μm DT ice (with a DT gas of 0.3 mg/cm^3 inside). By applying the Spitzer model and present fitted model for K_e, the density (normalized by 500 g/cm^3) and temperature (normalized by 1000 eV) profiles at the stagnation stage ($\sim$31 ns after the main pulse) are shown in Fig. 6. Prominently, it is indicated that the density of the DT fuel is more compressed (by about 3%), and the temperature in the hot-spot region is even more enhanced (by about 13%) with our present model [Eq. (7)]. This is physically reasonable by the fact shown in Fig. 3(a) that the classical Spitzer model fundamentally underestimates the electronic thermal conductivity in the partially degenerate regime, which turns out to substantially influence different kinds of heat transport during the implosion, as shown in Fig. 6.

IV. CONCLUSION

In summary, we have determined the EOS and transport coefficients of DT plasmas within QMD simulations in the hot dense regime as reached in future ICF experiments. The wide range EOS has been built from the coupled to the kinetic regime to describe pressures up to 10^6 Mbar. A clear chain of simulations in computing the thermophysical properties of hot dense plasma has been demonstrated. The ionic diffusion coefficient and viscosity have been simulated and compared to various OCP model simulations. The electronic and radiative thermal transport coefficients have also been determined, clearly showing different weights when crossing different pressure-temperature regimes. The ability to simulate these parameters in a self-consistent way shown by our results opens aa alternative way to validate the classical theoretical models currently used in hydrodynamical simulations for ICF.

ACKNOWLEDGMENTS

This work was supported by the NSFC under Grants No. 11275032, No. 11005012, and No. 51071032; by the National Basic Security Research Program of China; and by the National High-Tech ICF Committee of China.

[1] S. Atzeni and J. Meyer-ter-Vehn, *The Physics of Inertial Fusion: Beam Plasma Interaction, Hydrodynamics, Hot Dense Matter*, International Series of Monographs on Physics (Clarendon, Oxford, 2004).

[2] J. D. Lindl, *Inertial Confinement Fusion: The Quest for Ignition and Energy Gain Using Indirect Drive* (Springer-Verlag, New York, 1998).

[3] S. H. Glenzer, B. J. MacGowan, P. Michel, N. B. Meezan *et al.*, Science **327**, 1228 (2010).

[4] S. H. Glenzer, B. J. MacGowan, N. B. Meezan, P. A. Adams *et al.*, Phys. Rev. Lett. **106**, 085004 (2011).

[5] S. X. Hu, B. Militzer, V. N. Goncharov, and S. Skupsky, Phys. Rev. Lett. **104**, 235003 (2010).

[6] J. L. Milovich, P. Amendt, M. Marinak, and H. Robey, Phys. Plasmas **11**, 1552 (2004).

[7] V. Recoules, F. Lambert, A. Decoster, B. Canaud, and J. Clérouin, Phys. Rev. Lett. **102**, 075002 (2009).

[8] J. Vorberger, I. Tamblyn, B. Militzer, and S. A. Bonev, Phys. Rev. B **75**, 024206 (2007).

[9] W. Lorenzen, B. Holst, and R. Redmer, Phys. Rev. Lett. **102**, 115701 (2009).

[10] M. A. Morales, L. X. Benedict, D. S. Clark, Eric Schwegler *et al.*, High Energy Density Phys. **8**, 5 (2012).

[11] J. Vorberger, D. O. Gericke, and W.-D. Kraeft, High Energy Density Phys. **9**, 448 (2013).

[12] B. Holst, R. Redmer, and M. P. Desjarlais, Phys. Rev. B **77**, 184201 (2008).
[13] B. Holst, M. French, and R. Redmer, Phys. Rev. B **83**, 235120 (2011).
[14] F. Lambert, J. Clerouin, and G. Zérah, Phys. Rev. E **73**, 016403 (2006).
[15] For details of ABINIT code, please refer to http://www.abinit.org.
[16] M. Brack and R. K. Bhaduri, *Semiclassical Physics* (Westview, Boulder, CO, 2003).
[17] C. Wang, X. T. He, and P. Zhang, Phys. Rev. Lett. **106**, 145002 (2011).
[18] The time steps have been taken as $\Delta t = a/20\sqrt{k_B T/m_i}$, where m_i is the ionic mass and a the mean ionic sphere radius written as $a = (3/4\pi n_i)^{1/3}$ with n_i the ionic number density.
[19] P. Debye and E. Hückel, Z. Phys. **24**, 185 (1923).
[20] S. X. Hu, B. Militzer, V. N. Goncharov, and S. Skupsky, Phys. Rev. B **84**, 224109 (2011).
[21] J.-Y. Dai, Y. Hou, and J.-M. Yuan, Astrophys. J. **721**, 1158 (2010).
[22] Y. Hou, F. Jin, and J.-M. Yuan, Phys. Plasmas **13**, 093301 (2006).
[23] I. Kwon, J. D. Kress, and L. A. Collins, Phys. Rev. B **50**, 9118 (1994).
[24] L. Collins, I. Kwon, J. Kress, N. Troullier, and D. Lynch, Phys. Rev. E **52**, 6202 (1995).
[25] J. G. Clérouin and S. Bernard, Phys. Rev. E **56**, 3534 (1997).
[26] J. D. Kress, J. S. Cohen, D. A. Horner, F. Lambert, and L. A. Collins, Phys. Rev. E **82**, 036404 (2010).
[27] J. P. Hansen, I. R. McDonald, and E. L. Pollock, Phys. Rev. A **11**, 1025 (1975).
[28] J. Daligault, Phys. Rev. Lett. **96**, 065003 (2006).
[29] H. Ohta and S. Hamaguchi, Phys. Plasmas **7**, 4506 (2000).
[30] T. Saigo and S. Hamaguchi, Phys. Plasmas **9**, 1210 (2002).
[31] $\kappa = k_D a$ is a dimensionless parameter with k_D^{-1} the screening length and a the interparticle distance.
[32] S. Bastea, Phys. Rev. E **71**, 056405 (2005).
[33] G. V. Chester and A. Thellung, Proc. Phys. Soc. London **77**, 1005 (1961).
[34] W. B. Hubbard, Astrophys. J. **146**, 858 (1966).
[35] Y. T. Lee and R. M. More, Phys. Fluids **27**, 1273 (1984).
[36] L. Spitzer and R. Härm, Phys. Rev. **89**, 977 (1953).
[37] S. Ichimaru and S. Tanaka, Phys. Rev. A **32**, 1790 (1985).
[38] G. Faussurier, C. Blancard, P. Cossé, and P. Renaudin, Phys. Plasmas **17**, 052707 (2010).
[39] F. Lambert, V. Recoules, A. Decoster, J. Clérouin, and M. Desjarlais, Phys. Plasmas **18**, 056306 (2011).
[40] Y. B. Zeldovich and Y. P. Raizer, *Physics of Shock Waves and High Temperature Hydrodynamic Phenomena* (Academic, New York, 1998).
[41] B. H. Armstrong, Astrophys. J. **136**, 309 (1962).
[42] W. Pei, Commun. Comput. Phys. **2**, 255 (2007).